Journal of Applied Chemistry JAC
http://chemistry.journals.semnan.ac.ir

Electrochemical Reduction of CO_2 Using Cu (II) and Ni (II) Complexes with 8-Hydroxyquinoline Ligand

Mohammad Reza Binaeizadeh[a], Ahmad Amiri[a,*], Farzaneh Fadaei[b], Kurt Schenk-Joß[c]

[a]*Department of Chemistry, College of Science, University of Tehran, Tehran, Iran.*
[b] *Institute of Chemical Sciences and Engineering, École Polytechnique Fédérale de Lausanne, CH-1015 Lausanne, Switzerland.*
[c]*Institute of Physics, École Polytechnique Fédérale de Lausanne, CH-1015 Lausanne, Switzerland.*

Article history:
Received: 09/Oct/2019
Received in revised form: 21/Nov/2019
Accepted: 11/Feb/2020

Abstract

Two dinuclear Cu (II) and Ni (II) complexes of the general formula $[Cu_2L_2]$, (**1**), and $[Ni_2L_6].4(C_2H_5OH)$, (**2**), which L=8-Hydroxyquinoline have been synthesized and characterized by elemental analysis, IR and UV-Vis spectroscopic methods. The crystal structure analysis showed the binuclear structure for **1** and the Cu (II) centers adopt a distorted square pyramidal geometries. Two Cu centers in complex **1** are linked via μ-O coordination bridge modes of 8-hydroxyquinoline ligands with the Cu-Cu distances of 3.534 Å. The electrochemical behavior of the free ligand and corresponding **1** and **2** complexes was studied in DMF. The cyclic voltammetry of the complexes **1** and **2** show an irreversible metal and ligand based reductions at negative potentials. The electrocatalytic activity of the complexes **1** and **2** was monitored for CO_2 reduction in DMF solution. The results show that the complexes can be used as new electrocatalysts for CO_2 reduction, leading to formation of carbon monoxide product.

Keywords: Copper (II) Complexes, Crystal Structure, Electrocatalyst, CO_2 Reduction.

1. Introduction

Carbon dioxide is the most notorious greenhouse gas, released by both natural and artificial processes. It is also a necessary material for the growth of all earth's plants and for many industrial processes. In an ideal scenario, the CO_2 produced on Earth should be balanced with what is consumed, so that the level of CO_2 remains constant to maintain environmental stability. Unfortunately, with the intensification of human industrial activities, this balance has gradually been disrupted, leading to more CO_2 production and making global warming a pressing issue. Therefore, reducing CO_2 production and converting CO_2 into useful materials seems to be necessary, indeed critical, for environmental protection, and various governments worldwide have signaled their concern by increasing their investment in research to address the CO_2 issue [1]. In recent years, CO_2 conversion using electrochemical catalysis approaches has attracted great attention for its several advantages: (1) the process is controllable by electrode potentials and reaction temperature; (2) the supporting electrolytes can be fully recycled so that the

*.**Corresponding author:** Assistant Professor of Inorganic Chemistry, University of Tehran, School of Chemistry, Tehran, Iran E-mail address:ahmadamiri@ut.ac.ir

overall chemical consumption can be minimized to simply water or wastewater; (3) the electricity used to drive the process can be obtained without generating any new CO_2 sources include solar, wind, hydroelectric, geothermal, tidal, and thermoelectric processes; and (4) the electrochemical reaction systems are compact, modular, on-demand, and easy for scale-up applications [2-4].

The electrochemical reduction of CO_2 usually requires a high potential of nearly -2 V vs. NHE for a one-electron process. By performing a two-electron or proton-coupled multi-electron CO_2 reduction, however, the required potential can be lowered significantly. In reality, the actual reduction potentials are much higher than the Nernst potential due to barrier induced overpotentials. For lowering the actual redox potential of the CO_2 reduction process, suitable electrocatalysts are required [5-8].

One the important products of the electrocatalysis reduction of CO_2 is CO, which can be exploited for introducing carbonyl functionalities into a plethora of molecules in both an academic and an industrial setting. Carbon monoxide is a key component in large industrial processes such as the Fischer–Tropsch synthesis of hydrocarbons or the Monsanto/Cativa acetic acid synthesis [9-11].

Concerning the generation of CO from carbon dioxide, metal complexes with Pyridine derivatives ligands are among the most promising candidates for homogeneous catalysis in terms of activities and lifetimes[12-14]. Up to now, mainly nickel- and copper-based systems have been reported for their ability to electrochemically accelerate the reduction of CO_2 to CO [14,15]. Because in these complexes nitrogen donor atoms in the backbones of pyridyl ligands can be bound to CO_2 in the form of carbonate [16,17].

One of the important pyridine ligands whose complexes with nickel and copper can be used as effective catalysts in reducing carbon dioxide is 8-hydroxyquinoline (8-HQ) ligand. The compound 8-hydroxyquinoline and its derivatives are of great importance in separation techniques, absorption spectroscopy, fluorometry and chromatography because they can form many complexes with a variety of metal ions [18]. Also, 8-hydroxyquinoline and its derivatives are active-redox ligands that are widely used due to the effective coupling of ligand orbitals with metal d-orbitals. Due to the presence of redox active ligand orbitals in complex boundary orbitals, these ligands participate in catalytic processes as electron sources [19,20].

Herein, we report the synthesis and characterization of two binuclear copper (II)and nickel (II) complexes. Crystal structures as well as the spectroscopic and results on electrocatalytic activity of these complexes in the reduction of CO_2 was also investigated.

2. Experimental procedure

2. 1 Materials and methods

All solvents and chemicals were of commercial reagent grade and used as received from Aldrich and Merck. Elemental analysis was performed with a Perkin-Elmer 2400II CHNS-O elemental analyzer. UV–visible spectra were recorded on a BS-UV-Vis1600 Spectrophotomether . Infrared spectra (KBr disks) were obtained with a WQF-510A FT-IR spectrophotometer. The ^{1}H-NMR spectra were obtained on a Bruker Avance III 400 MHz spectrometer. Cyclic voltammograms were recorded by use of a SAMA 500 Research Analyzer.Three electrodes were used in this system, a glassy carbon working electrode, a platinum disk auxiliary electrode, and Ag wire as reference electrode. The glassy carbon working electrode (Metrohm 6.1204.110) with 2.0 ± 0.1 mm diameter was manually cleaned with 1 lm alumina polish before each scan. Tetrabutylammonium hexafluorophosphate (TBAH) was used as supporting electrolyte. The solutions were deoxygenated by purging with Ar for 5 min. All electrochemical potentials were calibrated vs. $Fc^{+/o}$ couple ($E° = 0.45$ V vs. SCE) as an internal standard under the same conditions [21].

Online test of gas-phase products was done on a gas chromatography (GC) equipped with a Carboxen 1010 PLOT capillary column and a thermal conductivity detector (VICI). Ar was used as carrier gas. The flow rate of CO_2 was set as 5 sccm.

2. 2 Synthesis of $[Cu_2L_2]$ (1)

A solution of 0.020 g $Cu(CH_3COO)_2.H_2O$ (0.1 mmol) in 10 cm^3 methanol was added dropwise to a solution of 0.030 g 8-HQ (0.2 mmol) in 10 cm^3 chloroform [22]. The final bright green crystals suitable for X-ray crystallography were obtained by slow evaporation of the solvent at room temperature. The crystals were isolated by filtration,washed with cold diethyl ether and dried under vacuum. Yield: 51%; Anal. Calc.: C, 61.45; H, 3.44; N, 7.96. Found: C, 61.20; H, 3.32; N, 7.36%. FT-IR (KBr, cm^{-1}): 3050 (C-H), 1110 (C-O stretch).UV–Vis (DMF): λ_{max} (nm) (ε, L mol^{-1} cm^{-1}): , 582 (116), 414 (10958), 338 (5591), 323 (4571).

2. 2 Synthesis of $[Ni_2L_6]$ (2)

A solution of 0.025 g $Ni(CH_3COO)_2.4H_2O$ (0.1 mmol) in 10 cm^3 ethanol was added dropwise to a solution of 0.030 g 8-HQ (0.2 mmol) in 10 cm^3 ethanol [23]. The final bright green crystals suitable for X-ray crystallography were obtained by slow evaporation of the solvent at room temperature. The crystals were isolated by filtration,washed with cold diethyl ether and dried under vacuum. Yield: 62%; Anal. Calc.: C, 63.72; H, 5.35; N, 7.19. Found: C, 62.90; H, 4.97; N, 6.73%. FT-IR (KBr, cm^{-1}):3039 (C-H stretch), 1108 (C-O), UV–Vis (DMF): λmax (nm) (ε, L mol^{-1} cm^{-1}): 409 (12508), 342 (16752), 530 (43).

Table 1. Crystal Data and Structure Refinement of **1** and **2**.

Formula	**$C_{36}H_{24}Cu_2N_4O_4$ (1)**	**$C_{54}H_{38}N_6Ni_2O_6{\cdot}4(C_2H_6O)$ (2)**
M	703.67	1168.59
crystal system	Monoclinic	Triclinic
space group	$P2_1/c$	$P\bar{1}$
a (Å)	10.6380 (5)	12.3231 (7)
b (Å)	8.6241 (3)	14.9243 (9)
c (Å)	15.2397 (8)	17.2989 (11)
α (deg)	90	64.820 (4)
β (deg)	102.204 (4)	83.487 (5)
γ (deg)	90	79.975 (5)
V ($Å^3$)	1366.54 (11)	2832.5 (3)
Z	2	2
μ (mm^{-1})	1.61	0.73
R(int)	0.025	0.100
total reflections	3680	15203
$I > 2\sigma(I)$	3306	8635
$R[F^2 > 2\sigma(F^2)], wR(F^2), S$	0.023, 0.072, 1.03	0.062, 0.173, 0.99

3. Results and Discussion

3. 1 Spectral Studies

The IR spectra of complexes **1** and **2** exhibit a moderately strong peak at 1597 and 1571 cm^{-1} corresponding to the -C=N stretching vibrations of coordinated 8-HQ ligand. The two absorption bands at 1110 and 1108 cm^{-1} for **1** and **2** are attributed to ν_{C-O} vibrations. The disappearance of the broad peak in the area 2500-3500 cm^{-1} in IR spectra of complexes confirm the coordination of the ligand to the metal ion center in its deprotonated form [24-26].

The electronic spectra of **1** and **2** were recorded in DMF. The electronic spectrum of five-coordinate di-copper(II) complex with a square-pyramidal geometry, **1,** (Fig. S1) shows four absorption bands; a weak d–d transition band at 582 nm (ε= 116 $M^{-1}cm^{-1}$), an intense transition band at 414 nm corresponding to the metal to ligand charge transfer (MLCT), and two ligand entered transirion peaks at 323 nm and 338 nm [27, 28]. The octahedral nickel(II) complex, **2**, shows a band at 530 nm with ε = 43 $M^{-1}cm^{-1}$ corresponding to ligand field transition (Fig. S2). An intense absorption band at 409 nm is attributed to MLCT and the higher energy band at 342 nm was assigned to an intraligand $\pi \rightarrow \pi^*$ transitions [27].

3. 2 Description of Structures

Crystal structural data of the complexes **1** and **2** are listed in Table 1. Independent reflection data were collected for **1** and **2**, with Mo Kα radiation at 292 K and 180 K by Diffraction Stoe IPDS II device system. The solving and refining of the crystal structure was performed using F2 SHELXL-2014/7 program.

All two structures are centrosymmetric dimers of metal ions, penta coordinated in **1** and hexa coordinated for **2.**

The molecular structure of **1** is shown in Fig. 1 and selected bond distances and angles are listed in Table S1. The complex **1** has a symmetrical structure belonging to space group P21/c. The copper atoms are five-coordinate in a square pyramidal environment, whose axial position is occupied by the oxygen atom O(2i) from the deprotonated 8-HQ ligand with the bond length of 2.8507(13) Å. As shown in Table S1, each Cu (II) center has a distorted square-pyramid geometry. The Cu1-N1 (1.9744 Å) and Cu1-N2 (1.9725 Å) bond lengths show a little difference (0.0017 Å), while this value for the two Cu1-O1 (1.9296) and Cu1-O2i (2.8507) is about 0.0093 Å.

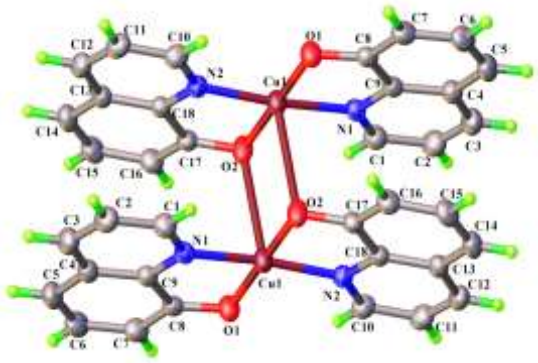

Fig. 1. Crystal structure of the complex **1**.

Deviation of the O2-Cu1-N2, (82.62°), and O1-Cu1-N1, (84.79°) bond angles from 90° confirm the existance of hinderence in the structure of the **1**. Also the O2-Cu-O2i bond angle is 1.1° as much as smaller than its exterior O1-Cu-O2i bond angle and confirm the the distorted dinuclear structure of the complex [29].

The molecular structure of **2** was shown in Fig.2. Complex **2** was crystallized in triclinic system with an octahedral geometry. The Ni1-O1 and Ni1-O3 bond lengths differencesare approximately 0.009 Å.

Selected bond distances and angles are given in Table S2. The O4—H4A (1.32 Å) , O6—H3A (1.36 Å), O1—H4A (1.12 Å) and O3—H3A (1.08 Å) bond distances in the $Ni_2O_2H_2$ and N2—Ni1—N3, N1—Ni1—O3, O2—Ni1—O1 bond angles are 164.13 (12)°, 168.74 (12)° and 173.12 (11)° respectively, deviate from 180 °. All the angles around the Ni(II) center have deviate significantly from 90°. The O2–Ni–Ni and N1–Ni–N3 have opened up to 96.40(12)° and 97.18(12)°, respectively, and the O2–Co–N2, N3-Ni-O3 and N1-Ni-O1 have reduced to 80.76(11)°, 79.36(10)° and 79.42(12)°. The Ni–O and Ni–N bond distances of 8-HQ are equal within the limits of experimental error.

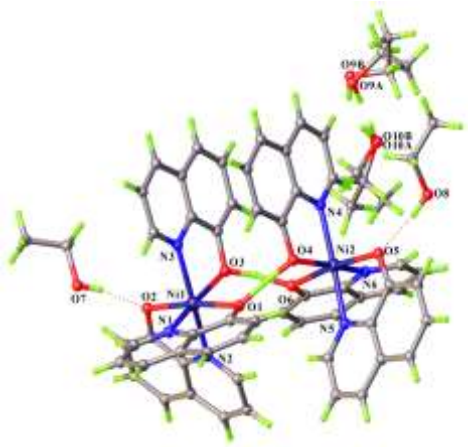

Fig. 2. Crystal structure of the complex **2**.

3. 3 Hirshfeld Surface Studies

The Hirshfeld surface surrounded a molecule is defined by points where the attempt to the electron density from the molecule of interest is equal to the contribution from all the other molecules [30]. For each point on that isosurface two distances are determined: one is de represents the distance from the point to the nearest nucleus external to the surface and second one is di represents the distance to the nearest nucleus internal to the surface [31]. The surfaces are shown as transparent to allow visualization of the **1** and **2** molecules around which they were calculated. The Hirshfeld surfaces of complexes **1** and **2** are shown in (Fig. S3) and (Fig. S4).

The deep red colour spots in di are strong interactions such as H…O (9.5%) and H…O (6.8%) for complexes **1** and **2** , respectively. Blue wheel in de (Fig. S3) that shows the interaction of the π-π interactions on the surface of the quinoline ring (C...C 16.0%). The shapeindex surface indicates the electron density surface shape around the molecular interactions [32]. The small range of area and light color on the surface

represents a weaker and longer contact other than hydrogen bonds.

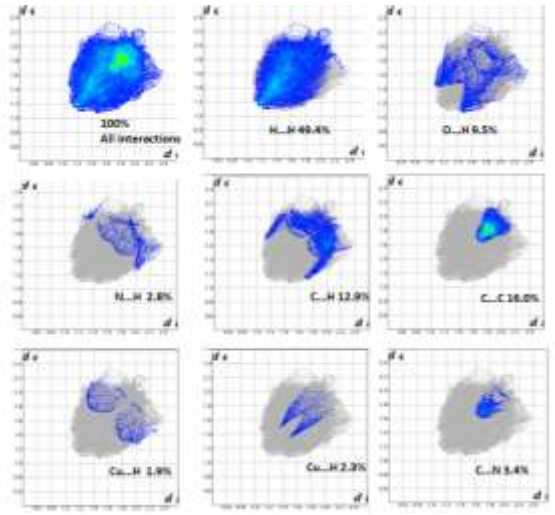

Fig. 3. Fingerprint plots representing quantity of molecular interactions in complex **1**.

The curvedness surface indicates the electron density surface curves around the molecular interactions. The two-dimensional fingerprint plots of complexes 1 and 2 exemplify the strong evidence for the intermolecular interactions pattern[33]. In the fingerprint region (Fig. 3), complexes 1, O…H and H…O (9.5%) interactions. Hydrogen bonding interactions H…H (49.4%) are very high compared to the other bonding interactions. Sharp curved spike at the bottom left area indicates the N…H and top left corner with curved spike indicates the H…N (2.8%). The finger print C…H and H…C(12.9%) interactions. The finger print at the top right area represents C…N and N…C (3.4%) interactions. Sharp curved spike at the center area indicates the C…C (16.0%) interactions.Two sharp curved spike at the center area indicates the Cu…O (2.3%) interactions,that Jahn-Teller effect shows.

In the fingerprint region of the complex **2**, O…H(3.0%) interactions are represented by a spike in the bottom area whereas the H…O (3.7%) interactions are represented by a spike in the top left region in the fingerprint plot (Fig.S5). Hydrogen bonding interactions H…H (57.7%) are very high compared to the other bonding interactions. The finger print C…H and H…C(28.9%) interactions. The finger print at the top right area represents H…N and N…H (2.0%) interactions. Sharp curved spike at the center area indicates the C…C (3.2%) interactions, the pattern of red and blue triangles on the same region of the shape index surface (Fig. S4) is characteristic of π–π stacking [34].

3. 3 Electrochemistry

The electrochemistry of the 8-HQ ligand and corresponding **1** and **2** complexes in DMF solutions in the presence of 0.1 M TBAH as supporting electrolyte were recorded at a glassy carbon working electrode under an argon atmosphere. The approximate concentrations of the compounds were 10^{-3}–10^{-5} M.

Electrochemical studies of ligands derived from pyridine and quinoline has by different research groups showed that these compounds are electroactive in the common potential ranges. The two reduction waves observed in the voltammogram of 8-HQ at -0.99 V and -1.93 V are attributed to an irreversible reduction of quinoline rings of the free 8-HQ ligand. (Fig.S6). The irreversibility of the reduction processes of the 8-HQ ligand in the potential ranges of 0.1 to -2.5 V is presumably due to the instability of the reduced species, resulting from addition of one electron to the already reduced ligand.

The cyclic voltammogram of **1** shown in Fig. 4 consists of an irreversible reduction waves in the potential ranges of -0.25 V to -2.03 V, corresponding to $Cu^{II/I}$, $Cu^{I/0}$ and ligand centered reductions. The high intense oxidative responses at +0.12 V and +0.19 V are attributed to the $Cu^{0/I}$, deposited on an electrode surface. of solid copper oxidation process are deposited on the electrode surface.

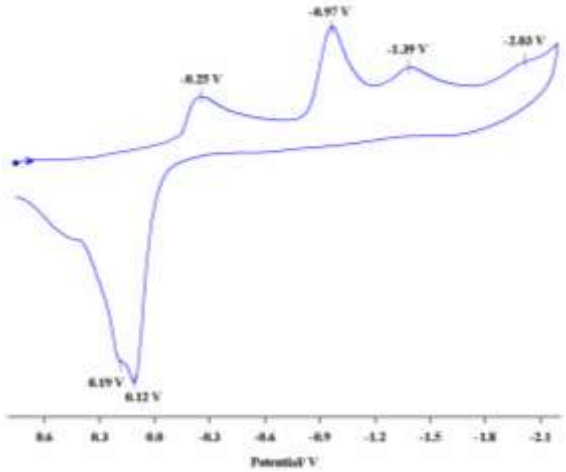

Fig. 4. Cyclic voltammogram of complex **1** in DMF and 0.1 M TBAH at 298 K, SR = 100 mV/S, c = 6.18×10^{-4} M.

The cyclic voltammogram of the Ni(II) complex **2**, (Fig. 5) shows an irreversible redox process at -1.45 V, corresponding to $Ni^{II/I}$ reduction. The reduction process observed at the potential ranes of -1.91 V to -2.25V, are attributed to the quinoline qings of the coordinated ligand.

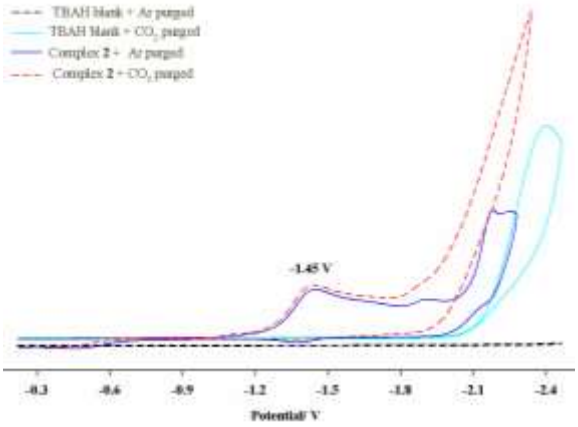

Fig. 5. Cyclic voltammograms of **2** in DMF under an Ar (blue) and CO_2 (red) atmosphere. SR = 100 mV/s.

3. 3 Electrocatalytic Studies

To investigate the electrocatalytic ability of the complexes **1** and **2** in the reduction of CO_2, the electrocatalytic behavior of **1** and **2** was studied in the peresence of CO_2, Fig.5. The results showed that complex **2** exhibited a better catalytic activity in electrochemical conversion of CO_2. This can be attributed to the more stability of **2** versus **1** during the electocatalytic process and beterr interactions between HOMO and LUMO molecular orbitals in **2** and carbon dioxide molecule during the electron transfer process in comparison with **1**.

The GC analysis indicated that the CO was detected as the gas-phase product (Fig.6). To evaluate the role of H_2O in the reduction of CO_2, 20 µl water was added to the electrolyte solution of **1** and **2** and their electrocatalytic activity was monitored. The results showed that H_2 and CO were detected as the products.

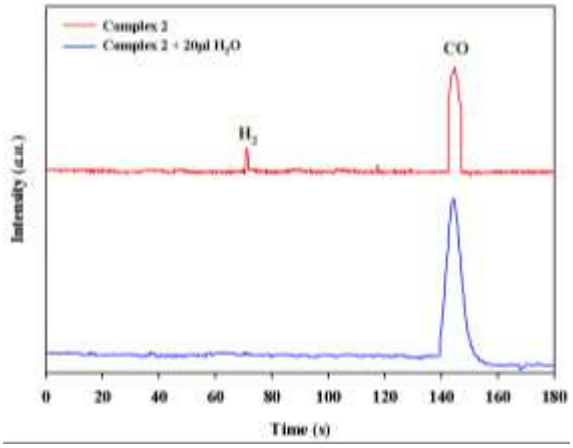

Fig. 6. GC analysis of a headspace sample of **2** after 1h electrolysis in absence and presence of 20 µl H_2O.

4. Conclusion

In this study, two binuclear Cu(II) (**1**) and Ni (II) (**2**), with the bidentate ligand L were synthesized and characterized by various spectroscopic methods. Single crystal X-ray diffraction studies of these complexes indicated that they had binuclear structures and environment around the copper centers in the complex **1** is distorted square pyramidal. The coordination geometry of Ni(II) in complex 2 was obtaines as distorted octahedral. Electrochemical studies of the complexes **1** and **2** in acetonitrile solution showed an electrochemically reversible reduction process corresponding to $Cu^{II/I}$, $Cu^{I/0}$ and $Ni^{II/I}$ metal centers in **1** and **2** respectively. The reduction peaks at the negative potential are attributed to the coordinated quinoline ligands. The presence of redox processes at negative potentials make these complexes as a candidate in electrocatalytic reduction processes. Electrocatalytic behaviour of these to complexes in CO_2 reduction was indicated the formation of CO in organic and also H_2 in the presence of H_2O.

Supplementary Informations

Crystallographic data for both complexes reported in this paper have been deposited at the Cambridge Crystallographic Data Centre (CCDC), under numbers CCDC 186247 (**1**) and 186123 (**2**). This information can be achieved free of charge from The Cambridge Crystallographic Data Centre at the following addresses: http://www.ccdc.cam.ac.uk.

Acknowledgments

The University of Tehran is gratefully acknowledged for the financial support of this research.This work has been supported by the Center for International Scientific Studies & Collaboration (CISSC).

References

[1] J. Hála, *J. Inorg. Nucl. Chem*. **27** (1965) 2659.

[2] L. M. Ramenskaya and O. V. Kraeva, *Russian. J. Phys. Chem.* **80** (2006) 90.

[3] S.C. Lee, M.I. Reed, X.Z. X. Zhan, E.G. Nelson, J.D. Lamb, P.B. Savage and J.S. Bradshaw, *Inorg. Chim. Acta*. **317** (2001) 174.

[4] A. Markus, M. Fiege and O. Osetska, *Coord. Chem. Rev*. **252** (2008) 812.

[5] R. Gustafson and A. E. Martell, *J. Am. Chem. Soc*. **81** (1959) 1033.

[6] D. Badocco, A. Dean, D.M. Valerio and P. Pastore, *Electrochimica Acta*. **52** (2007) 7920.

[7] Spence, J. T. and Ellis R. Peterson, i*norg. Chem.* **1** (1962) 277.

[8] Soroka, Krystyna, Rathnapala S. Vithanage, Denise A. Phillips, Brian Walker and Purnendu K. Dasgupta, *Anal. Chem*. **59** (1987) 629.

[9] Borrel, Marcel and René A. Pâris, *Analytica Chimica Acta*. **6** (1952) 389.

[10] Bratzel, M. P., J. J. Aaron, J. D. Winefordner, S. G. Schulman and Herman Gershon, *Anal. Chem*. **7** (1972) 1240.

[11] Chakrabarty, Manoj R., Edward S. Hanrahan, Ned D. Heindel and Golden F. Watts, *Anal. Chem*. **39** (1967) 238.

[12] Yamato Masatoshi, Kuniko Hashigaki, Yoshiko Yasumoto, Junko Sakai, Richard F. Luduena, Asok Banerjee, Shigeru Tsukagoshi, Tazuko Tashiro and Takashi Tsuruo, *J. Med. Chem.* **30** (1987) 1897.

[13] Singh Prabhpreet and Subodh Kumar, *Tetrahedron Lett*. **47** (2006) 109.

[14] J. P.Phillips, *Chem. Rev.* **56** (1956) 271.

[15] E.Pattison Scott and Michael F. Dunn, *Biochemistry*, **15** (1976) 3691.

[16] Zang Zhaoxia, Jerald S. Bradshaw, Xian X. Zhang, Paul B. Savage, Krzysztof E. Krakowiak, N. Kent Dalley, Ning Su, R. Todd Bronson and Reed M. Izatt, J. Org. Che*m.* **64** (1999) 3162.

[17] Zhujun, Zhang and W. Rudolf Seitz, *Anal. Chim. Acta*. **171** (1985) 251.

[18] Le Bahers, Tangui, Carlo Adamo and laria Ciofini, *Chem. Phys. Lett*. **472** (2009) 30.

[19] Haj Mohammad Abul, Miguel Quirós, Juan M. Salas, José A. Dobado, José Molina Molina, Manuel G. Basallote and M. Angeles Mánez, *Eur. J. Inorg. Chem*. **200** (2002) 811-818.

[20] DuBois, Daniel L, *Inorg. Chem* **53** (2014) 3935.

[21] N.G. Connelly and W.E. Geiger, *Chem Rev*. **96** (1996) 877.

[22] S. Meghdadi, M. Amirnasr, S.B.H. Moein Sadat, K. Mereiter and A. Amiri, *Monatsh Chem*. **145** (2014) 1583.

[23] M. Salavati-Niasari and A. Amiri, *Applied Catal. A*. **290** (2005) 46.

[24] Chapman, L. Ross and Robert S. Vagg, *Inorg. Chim. Acta*. **33** (1979) 227.

[25] J. C. Fanning and H. B. Jonassen, *Journal of Inorganic and Nuclear Chemistry*. **25** (1963) 29.

[26] Wei Chen and Yadong Li, *Cryst. Growth. Design*. **8** (2008) 564.

[27] Lorena M. A. Monzon and J. M. D. Coey, *J. Phys. Chem*. **119** (2011) 9182.

[28] Thummel, M., *Inorg. Chem*. **50** (2011) 10966.

[29] Van Albada, G.A., Wilberth JJ Smeets, Anthony L. Spek and Jan Reedijk, *Inorganica Chimica Acta*. **260** (1997) 151.

[30] Jayatilaka, *Cryst. Eng. Comm*. **11** (2009) 19.

[31] V. Meenatchi, *RSC Adv*. **5** (2015) 71076.

[32] Adam D. Martin, J.B., Timothy L. Easun, Alexander J. Blake, William Lewis and Martin Schroder, *Cryst. Growth Design*. **15** (2015) 1697.

[33] S.C. Hunter, C.M. Hoffmann, X. Wang, Yu-Sh. Chen, G.J. McIntyre and Zi-Li. Xue, *Inorg. Chem*. **53** (2014) 11552.

[34] M. Prankrishna, S.K.S., Amrita, J. Hemming, R. Prendergast, M. Helliwell, S.R. Choudhury, A. Frontera and S. Mukhopadhyay, *Inorg. Chem*. **51** (2012) 3557.